Monthly Weather Review
VOLUME 99, NUMBER 10
OCTOBER 1971

UDC 551.588.2:551.511.2

# AN ANALYSIS OF KINEMATIC VERTICAL MOTIONS

PHILLIP J. SMITH
Department of Geosciences, Purdue University, Lafayette, Ind.

## ABSTRACT

Several techniques exist for computing vertical motions. In this paper, radiosonde wind observations are used to compute vertical motions by the kinematic method. The presence of cumulative bias errors necessitates adjustment techniques. Simple tests of two techniques indicate that, for the period of this study, a divergence adjustment that is a function of pressure yields the best adjusted vertical motion fields. Further analysis shows that the adjusted estimates correlate well with observed synoptic features. Finally, comparison with estimates by the numerical method indicates that adjusted kinematic vertical motion fields are comparable.

## 1. INTRODUCTION

One of the most elusive of the parameters required in diagnostic and prognostic studies of the atmosphere is the vertical motion. Vertical motions exert a profound influence on the distribution of clouds and on the occurrence of precipitation. They provide the mechanism for vertical transport of any atmospheric property and thus influence the distribution of mass, momentum, and energy. Further, their relevance to energy processes has been established by White and Saltzman (1956) in their study of the role of vertical motion in the conversion of potential to kinetic energy.

Unfortunately, consistent estimates of vertical velocities have proven difficult to obtain. In cases where these velocities are comparatively large (e.g., thunderstorms), some direct measurements have been made (Battan 1964). But in synoptic scale and planetary scale systems, motions in the vertical are no more than a few centimeters per second and are therefore too small for reliable measurement. For these systems, it is necessary to estimate the vertical motion field using various computational methods applied to data gathered on other parameters. The techniques used have been summarized by Miller and Panofsky (1958) as the precipitation, kinematic, adiabatic, vorticity, and numerical methods. In addition, Danielsen (1966) has reported on vertical motion computations utilizing isentropic trajectories. Those methods used most extensively have been the kinematic, adiabatic, and numerical. Note that, although the true vertical velocity is defined by $w=dz/dt$, most recent studies utilize constant pressure coordinates and thus compute a pseudovertical motion, omega, defined by $\omega=dp/dt$. The two are related approximately by

$$\omega \simeq -\rho g w.$$

Each of the computational methods has certain inherent advantages and disadvantages. The adiabatic method (Panofsky 1951) utilizes the thermodynamic equation under the assumption of adiabatic flow to derive a vertical velocity equal to the adiabatic temperature change divided by the difference between the actual and adiabatic lapse rates. This possesses the advantage of a simple mathematical formulation with the complex effects of adiabatic heating eliminated by assumption. The adiabatic technique is hampered by the lack of temperature data more frequent than at 12-hr intervals, which can lead to nonrepresentative local temperature derivatives. Its application is also compromised when the actual lapse rate approaches the dry adiabatic or when diabatic heating is significant. Further, Wiin-Nielsen (1964) suggests that energy conversion estimates obtained by this method represent the difference between the actual conversion and the diabatic generation of available potential energy.

The numerical method has many variations. Fundamentally, the diagnostic relation for this method is derived by eliminating time derivative terms between the vorticity and thermodynamic equations, yielding the so-called "omega equation." The complexity of this equation depends on the extent of the assumptions made during its derivation, varying from the relatively simple quasi-geostrophic model (Thompson 1964, O'Neill 1966, Krishnamurti 1968*a*) to the complete linear balance model presented by Krishnamurti (1968*a*). The numerical method has provided consistent estimates of vertical motion for many years and has played an important role in numerical weather prediction models (Ellsaesser 1960, Cressman 1963). A particular advantage is that geostrophic or balanced wind formulations can be utilized, thus eliminating the need to use actual measured winds. The method also avoids the cumulative bias errors discussed below for the kinematic method. In the author's view, its disadvantages may be separated into two categories. If a more exact formulation of the omega equation is used, one is faced with the formidable task of providing independent estimates of processes such as diabatic heating and friction. The alternative is to assume that these and perhaps other processes are negligible. While this renders a simpler model, it also places some limitation on the scales of motion that might be adequately described. For example, Krishnamurti and Moxim (1971) provide estimates of $\omega$ for the occluded cyclone studied by Krishnamurti (1968*b*). Their results show upward motion maxima from their more complex model, including friction, sensible and latent heating, and a number of other processes, to be approximately twice the corresponding quasi-geostrophic values. This could have considerable impact on estimates of the energy balance of a well-developed cyclone. Danard (1964) found that the contribution to the vertical motion from the release of latent heat resulted in values for the release of potential energy which were 50 percent larger than those due to quasi-geostrophic values.

The kinematic method, as described by O'Brien (1970), utilizes the continuity equation in pressure coordinates to represent $\omega$ at a pressure level $p$ by

$$\omega_p=\omega_{p+\Delta p}+D_p \tag{1}$$

where

$$D_p=\int_p^{p+\Delta p} \nabla\cdot\mathbf{V}dp, \tag{2}$$

$\mathbf{V}$ is the horizontal wind vector, and $\nabla$ is the del operator on a constant pressure surface. The primary advantage of this method lies in the mathematical simplicity of eq (1), derived with hydrostatic balance as its only physical assumption. However, it does possess a serious disadvantage which has, no doubt, deterred its use in the past. Because of the basic dependence of the kinematic method on the divergence field, the method cannot be applied using a simplified nondivergent representation of the wind. Rather, it is necessary to utilize actual horizontal wind data. Errors in these data as well as inaccurate computing techniques often lead to biased divergence estimates. From eq (1), $\omega$ at a level $k$ is given by

$$\omega_k=\omega_{k-1}+D_k. \tag{3}$$

Defining $\omega_0$ as the value at the lower boundary, then

$$\omega_k=\omega_0+\sum_{i=1}^{k} D_i. \tag{4}$$

In this summation process, the bias errors in each $D_i$ tend to accumulate, producing unrealistic estimates of $\omega_k$ in the upper troposphere.

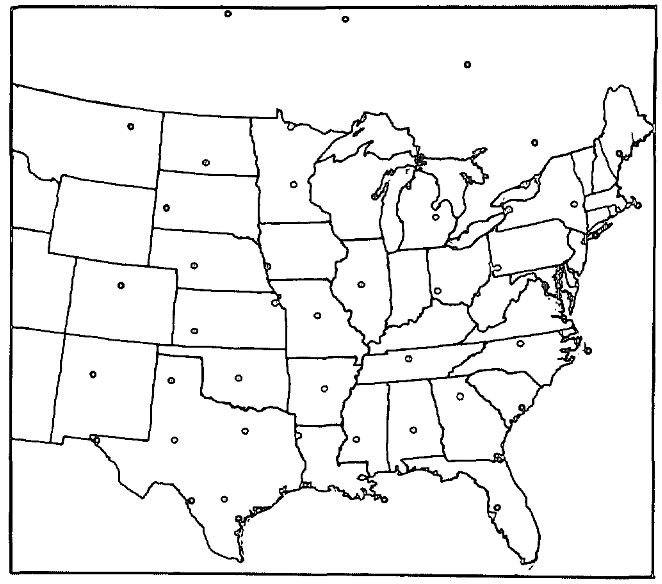

FIGURE 1.—Radiosonde stations utilized for vertical motion computations (closed circles) and as additional boundary stations (open circles).

A solution to this problem can come from one of two directions. The most obvious solution would be to devise a numerical technique which yields unbiased divergence estimates. Admitting the difficulty of this approach, the alternative is to seek techniques for adjusting the doubtful $\omega$ values. O'Brien (1970) has discussed the theoretical bases for several of these techniques. Also, adjustments have been applied to kinematic vertical motions in recent work by Krietzberg (1968), Lateef (1967), and Fankhauser (1969). The fundamental goal of this paper is to examine two of these techniques. For a single period of cyclone development, the author seeks to establish which of the adjustments tested provides the "best" estimates of $\omega$. These results are then examined to establish their correlation with observed synoptic scale events. Finally, some comparisons are made between the author's computations and those obtained using the numerical method.

## 2. DATA AND BASIC VERTICAL MOTION COMPUTATIONS

The data for this study consisted of upper air radiosonde wind observations (50-mb intervals for 0000 and 1200 GMT) for the network of stations shown in figure 1. This network provided data for vertical motion estimates at a maximum of 29 stations (black dots in fig. 1). The period of the study was 0000 GMT March 18, through 0000 GMT March 22, 1962. The evolution of the synoptic situation during this period is depicted in figures 2 and 3. The raw data[1] were obtained from the MIT General Circulation Data Library and the National Climatic Center.

Because of incomplete data coverage at high levels, only data obtained at or below 250 mb were utilized. Where

[1] Processed by Travelers Research Center, Inc., under National Science Foundation Grants GP 820 and GP 3657

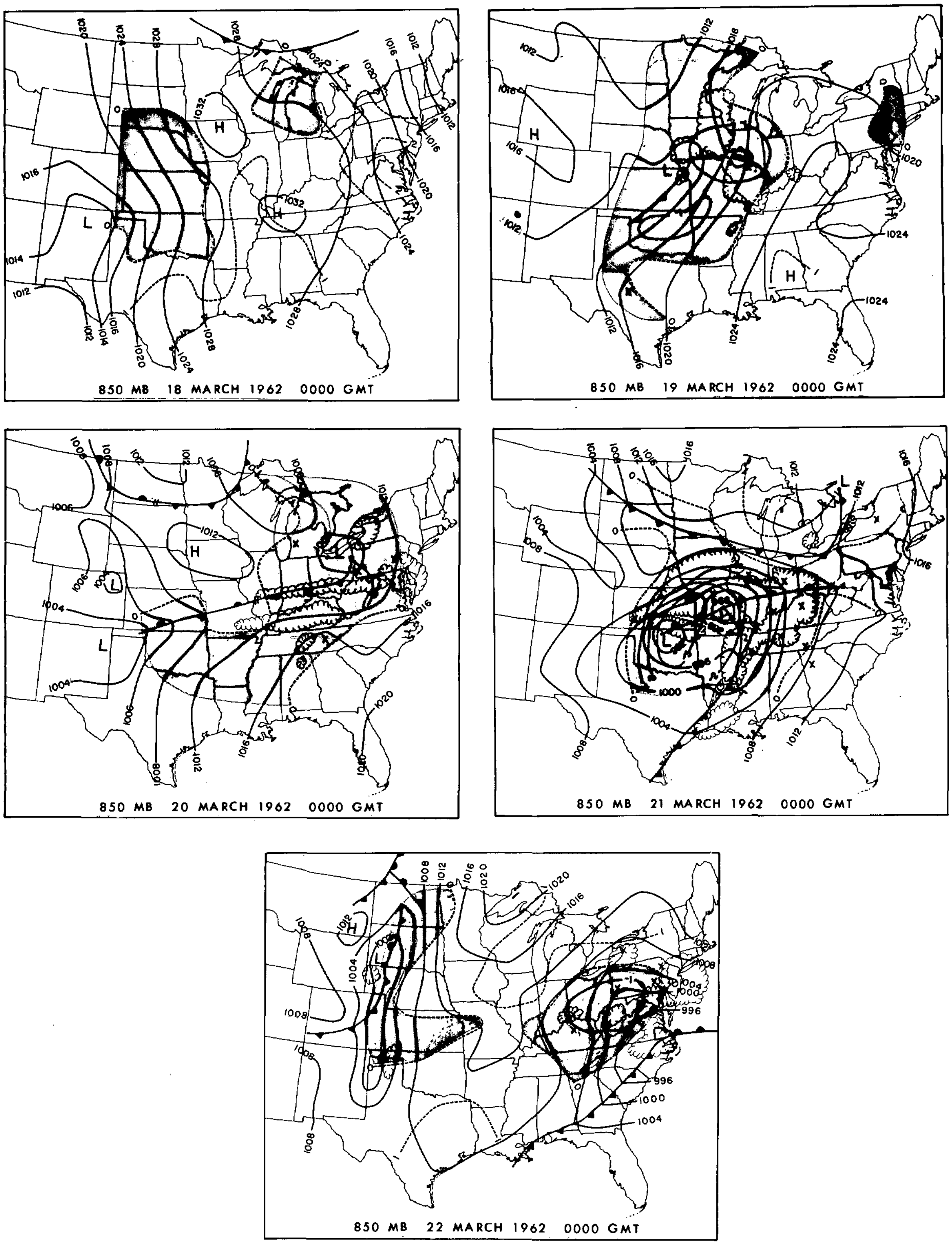


FIGURE 2.—Vertical motions at 850 mb (dashed lines, $\mu$bar/s) and surface synoptic features with regions of upward motion indicated by shading, radar depictions by wavy lines, and precipitation occurrences by Xs.

possible, missing data below 250 mb were estimated by linear interpolation. However, missing data were occasionally so extensive that $\omega$ could not be estimated at a few stations. The number of stations for which computations were made at each map time is given in table 1. The influence of missing data on the final results is noted later. To suppress the effects of random errors, the wind data were filtered using a five-point "least squares" approximating polynomial (Bullock et al. 1969).

Estimates of $D_k$ were made by rewriting eq (2) in the finite-difference form

$$D_k = \left[ \frac{(\nabla \cdot \mathbf{V})_k + (\nabla \cdot \mathbf{V})_{k-1}}{2} \right] (p_{k-1} - p_k) \tag{5}$$

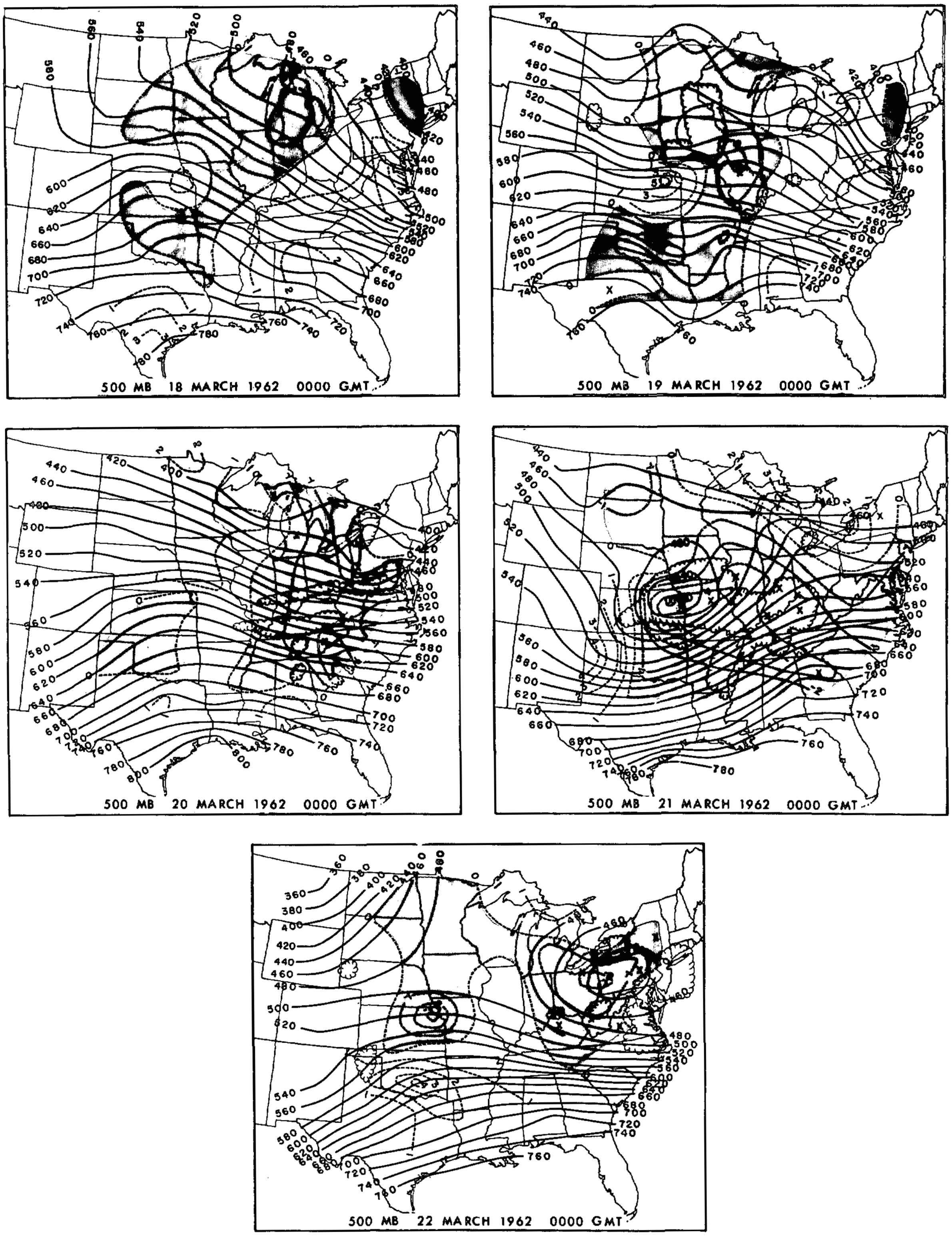


FIGURE 3.—Vertical motions at 500 mb (dashed lines, $\mu$bar/s) and 500-mb geopotential height contours (m, initial 5 omitted). Other features are the same as in figure 2.

where $\nabla \cdot \mathbb{V}$ was computed by the technique described by Smith et al. (1967). Briefly, this involves writing the $u$ and $v$ components of $\mathbb{V}$ at each station in terms of local two-dimensional truncated Taylor's series, retaining the two first-order derivatives and the second-order cross derivative. A set of these expressions is then used to produce a least-squares solution for the appropriate first-order derivatives. If one assumes that the wind velocity at the lower boundary (earth's surface) is zero, the lower boundary conditions become

$$(\nabla \cdot \mathbb{V})_0 = 0$$

and

$$\omega_0 = \frac{\partial p_s}{\partial t}$$

TABLE 1.—*Number of stations (N) for which vertical motion computations were made in 1962*

| | GMT | N |
|---|---|---|
| March 18 | 0000 | 28 |
| | 1200 | 28 |
| March 19 | 0000 | 27 |
| | 1200 | 27 |
| March 20 | 0000 | 24 |
| | 1200 | 21 |
| March 21 | 0000 | 22 |
| | 1200 | 21 |
| March 22 | 0000 | 24 |

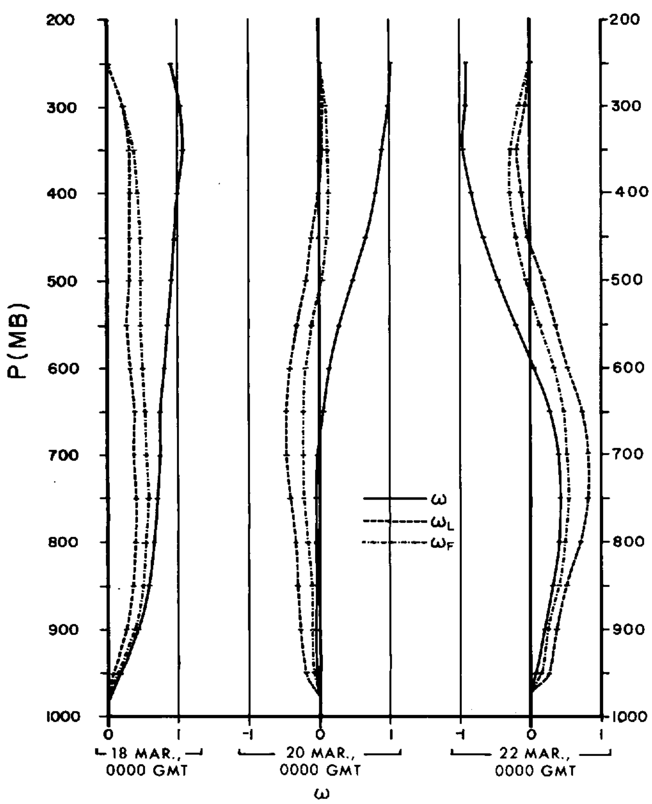


FIGURE 4.—Area average profiles of $\omega$, $\omega_L$, and $\omega_F$ ($\mu$bar/s).

where $p_s$ is the surface pressure. The local time derivatives were estimated by 24-hr centered finite differences. Finally, $\omega$ was computed at each of the 50-mb increments and averaged over all stations for each map time.

## 3. ADJUSTED VERTICAL MOTIONS

Smith and Horn (1969) have shown that, when averaging over a long time period (March 1962) and a large area (North America), a reasonable profile of $\omega$ can be obtained using the techniques applied in this study. However, when $\omega$ profiles for one map time are averaged over the smaller area considered in this paper, evidence of cumulative bias errors begins to appear. Figure 4 shows the area average $\omega$ profiles for March 18, 20, and 22, 0000 GMT. Obviously, profiles at individual stations also contain errors due to cumulative bias. It is apparent therefore that, in order to render these estimates useful, some corrections must be applied.

Several adjustment techniques are developed in a recent paper by O'Brien (1970). Because of their basic simplicity and because they have proved successful in other computational studies, the author chose two of these techniques for testing. The first, $\omega_L$, applied by Lateef (1967), yields a corrected vertical motion $\omega_k'$ given by

$$\omega_k' = \omega_k - \frac{k}{K}(\omega_K - \omega_T) \tag{6}$$

where $K$ is the integer value for the top level, $\omega_K$ is the computed value at $K$, and $\omega_T$ is an assumed correct value at the top of the column. Thus, $\omega_K - \omega_T$ becomes the cumulative error in $\omega$. This linear distribution of the error is described in O'Brien's discussion of the second-order adjustment scheme, which, as pointed out by Lateef, is equivalent to adjusting the divergence at every level by a constant. The second technique, $\omega_F$, proposed by O'Brien and used by Fankhauser (1969), produces an estimate of $\omega_k''$ given by

$$\omega_k' = \omega_k - \frac{k(k+1)}{K(K+1)}(\omega_K - \omega_T). \tag{7}$$

In this case, the equivalent divergence adjustment is a linear function of pressure, a more reasonable model because wind measurements tend to deteriorate with increasing height (Duvedal 1962).

The effect of these schemes is seen in figure 4 where the area averages of adjusted $\omega$ values are plotted with the original $\omega$ computations. Vertical motions adjusted by the first and second techniques are identified as $\omega_L$ and $\omega_F$, respectively. Note that $\omega_F$ reflects a less severe adjustment than $\omega_L$. The correct value at the top ($\omega_T$) was assumed to be zero. Since the top level (250 mb) is near the average tropopause level of 212 mb for this period and since $\omega_0$ is small, the upper level boundary value assumption is essentially equivalent to assuming that the vertically integrated divergence through the troposphere is zero.

The ability of $\omega_L$ and $\omega_F$ to improve $\omega$ was assessed by analyzing the relationship of the three estimates to cloud cover and precipitation in a manner analogous to that of Miller and Panofsky (1958). Hand analyses of 600-mb vertical motions were made for each map time. Values of $\omega$, $\omega_L$, and $\omega_F$ at synoptic reporting stations were then read off and compared with observed total cloud cover and precipitation. Because of uncertainties in cloud height information and because the final results were used primarily for comparative purposes, no attempt was made to distinguish cloud conditions occurring near 600 mb. Table 2 presents a summary of these results, prepared from a total of 633 surface observations. The numbers in parentheses represent the number of cases of zero to 3/8 (0–3) cloud cover, 7/8 to 8/8 (7–8) cloud cover without precipitation, and precipitation (Precip.) for each vertical motion category. Analysis of 4/8 to 6/8 cloud cover did not add any useful information and is therefore not included. The numbers adjacent to the parentheses represent the percent frequency of each weather class in their respective categories. Table 3 is the percent occurrence of upward motion for each weather class.

TABLE 2.—*Percentage and actual (in parentheses) occurrence of weather classes for various vertical motion categories. Upward motion is indicated by a minus sign. Units for vertical motion are μbar/s. Here, 0–3 = 0 to 3/8 cloud cover, 7–8 = 7/8 to 8/8 cloud cover without precipitation, precip. = precipitation occurrence.*

| | | $\omega \leq -3$ | $-3<\omega\leq -2$ | $-2<\omega\leq -1$ | $-1<\omega<0$ | Total up | $0\leq\omega<1$ | $1\leq\omega<2$ | $2\leq\omega<3$ | $3\leq\omega$ | Total down |
|---|---|---|---|---|---|---|---|---|---|---|---|
| $\omega$ | 0–3 | 16 (9) | 14 (6) | 23 (15) | 41 (43) | 27 (73) | 50 (66) | 63 (83) | 37 (22) | 51 (22) | 53 (193) |
| | 7–8 | 42 (23) | 56 (24) | 65 (42) | 50 (53) | 53 (142) | 45 (57) | 31 (41) | 52 (31) | 33 (14) | 40 (143) |
| | | }84 | }86 | }77 | }59 | }73 | }50 | }37 | }63 | }49 | }47 |
| | Precip. | 42 (23) | 30 (13) | 12 (8) | 9 (9) | 20 (53) | 5 (8) | 6 (7) | 11 (7) | 16 (7) | 7 (29) |
| $\omega_L$ | 0–3 | 16 (4) | 19 (7) | 38 (28) | 35 (54) | 32 (93) | 49 (96) | 51 (54) | 56 (14) | 47 (9) | 50 (173) |
| | 7–8 | 32 (8) | 54 (20) | 43 (32) | 42 (75) | 47 (135) | 45 (87) | 40 (42) | 44 (11) | 53 (10) | 44 (150) |
| | | }84 | }81 | }62 | }65 | }68 | }51 | }49 | }44 | }53 | }50 |
| | Precip. | 52 (13) | 27 (10) | 19 (14) | 23 (25) | 21 (62) | 6 (11) | 9 (9) | 0 (0) | 0 (0) | 6 (20) |
| $\omega_F$ | 0–3 | 12 (4) | 20 (7) | 16 (13) | 42 (59) | 29 (83) | 51 (84) | 56 (73) | 50 (17) | 60 (9) | 53 (183) |
| | 7–8 | 32 (11) | 43 (15) | 67 (54) | 47 (66) | 50 (146) | 42 (69) | 40 (52) | 39 (13) | 33 (5) | 41 (139) |
| | | }88 | }80 | }84 | }58 | }71 | }49 | }44 | }50 | }40 | }47 |
| | Precip. | 56 (19) | 37 (13) | 17 (14) | 11 (15) | 21 (61) | 7 (12) | 4 (5) | 11 (13) | 7 (1) | 6 (21) |

TABLE 3.—*Percentage occurrence of upward motion for indicated weather classes.*

| | $\omega$ | $\omega_L$ | $\omega_F$ |
|---|---|---|---|
| 0–3 | 27 | 35 | 31 |
| 7–8+precip. | 53 | 54 | 56 |
| Precip. | 65 | 76 | 74 |

TABLE 4.—*Comparative scores for vertical motion versus weather class. Higher values indicate higher correlations.*

| | Score | | Score | | Score |
|---|---|---|---|---|---|
| $\omega$ | 11 | $\omega$ | 6 | $\omega_L$ | 9 |
| $\omega_L$ | 11 | $\omega_F$ | 15 | $\omega_F$ | 12 |

In general, one would expect to find higher percentages of upward motion in classes 7–8 and Precip., and downward motion in 0–3. This is indeed the case in most categories. To provide objective evidence of the relative performance of each set of vertical motion estimates, percentage values for $\omega$, $\omega_L$, and $\omega_F$ were compared in pairs by the following procedure:

1. Considering weather classes Precip. and the sum of 7–8 and Precip., [(7–8) + precip.], one point each was given for the vertical motion estimate with the largest percent in the upward motion categories and the smallest percent in the downward motion categories, table 2; and
2. One point each was given for the largest total percent up in classes Precip. and (7–8) + precip. and the smallest total percent up in class 0–3, table 3.

The comparative scores are given in table 4. This simple test indicates that, for the period of this study, $\omega_F$ values give the best general correlation with observed weather, confirming O'Brien's view that the second adjustment technique is more realistic than the first.

## 4. COMPARISON WITH SYNOPTIC FEATURES

The test described in the previous section indicates that, for this data period, vertical motions derived from the second adjustment technique, $\omega_F$, are in general superior to $\omega$ and $\omega_L$. Examination of the relationship between $\omega_F$ and observed synoptic features is necessary to assess the overall utility of the $\omega_F$ estimates. Of course, any number of comparisons are possible. To conserve space, the author has chosen to restrict the discussion largely to 850-mb vertical motion and sea-level pressure fields (fig. 2), 500-mb vertical motion and geopotential height fields (fig. 3), and cross sections of vertical motion and relative humidity at 0000 GMT, March 18 and 21 (fig. 5). Included on the 850- and 500-mb charts are precipitation occurrences from synoptic reporting stations and radar depictions from the National Meteorological Center (NMC) facsimile radar charts. Sea-level pressure and frontal analyses were also taken from NMC charts. Height fields at 500 mb were carefully analyzed by the author in 20-m increments in order to capture the smaller scale minor wave features.

On March 18, high pressure dominated most of the region, with a weak Low developing over northeastern New Mexico. Through March 19 and 20 the anticyclone moved southeastward while the cyclone moved northeastward and eastward. The Low continued to deepen until the intermediate map time of 1200 GMT on the 19th, but never reached major proportions. On the 20th a new Low appeared over New Mexico. Through this period the 500-mb pattern was dominated by minor waves, exhibiting no major development. In general, the vertical motion fields correlate well with synoptic features. Low-level subsidence moved southeastward with the surface High. Upward motions at both levels propagated with the surface Low, increased in magnitude as the Low deepened, and finally decreased as development ceased. A maximum value of −3.4 μbar/s at 500 mb occurred at 1200 GMT, March 19. Notable also is the subsidence following the Low, reaching 500-mb values of 5.9 μbar/s at 0000 GMT, March 19 and 7.3 μbar/s at 1200 GMT. In the absence of prominent surface features, 500-mb vertical motions can usually be explained by minor waves, as evidenced by the location of zero lines near minor wave trough and ridge lines. Note the prominence of radar areas and precipitation in regions

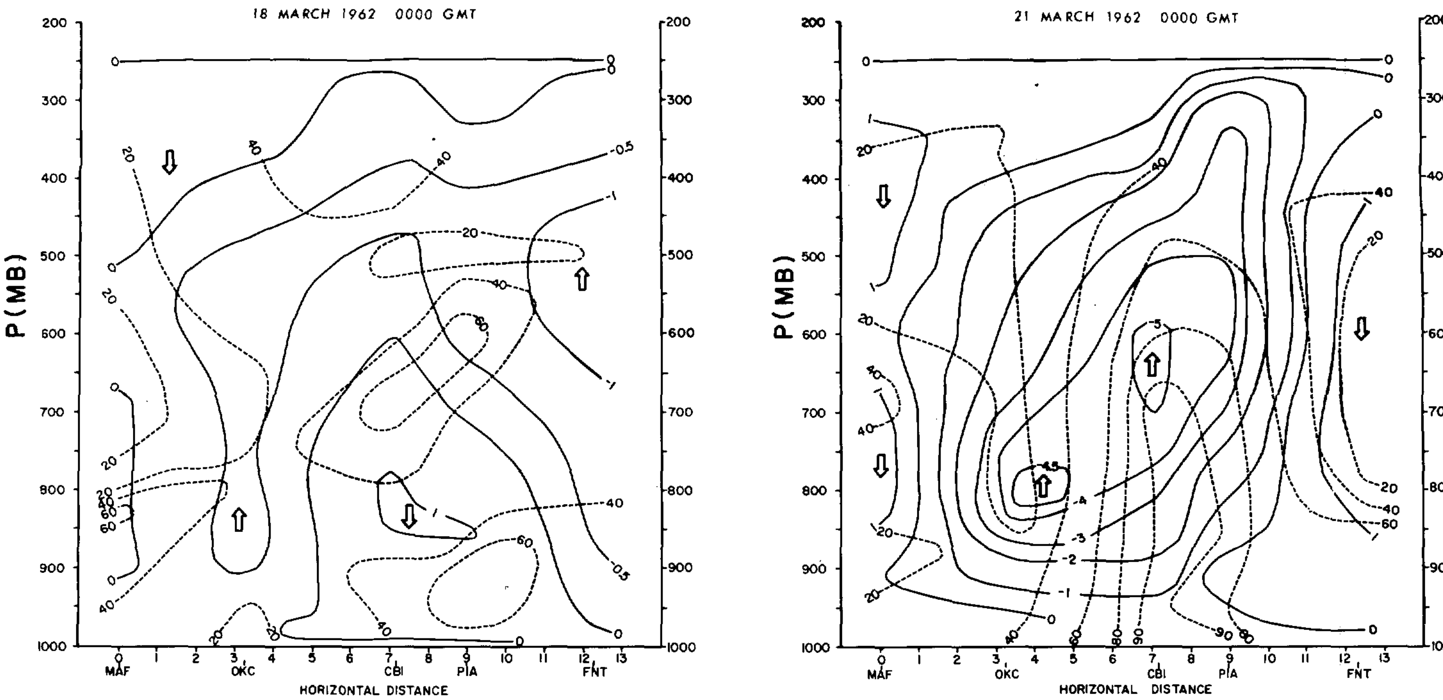


FIGURE 5.—Cross sections of vertical motion (solid lines) and relative humidity (dashed lines).

of upward motion, particularly those regions with $\omega_F$ greater than $-1$ $\mu$bar/s.

The new surface Low appearing over New Mexico at 0000 GMT, March 20 developed rapidly in the next 24 hr. By the 21st, the original Low had occluded and a second well-developed cyclone had appeared on the point of the occlusion. This second Low then moved eastward with little change in intensity until 0000 GMT on the 22d. The 500-mb flow for this period was marked by a prominent wave with closed cyclonic circulation. Once again the vertical motions show good agreement with synoptic features. Upward motion maxima of $-4.5\mu$bar/s and $-9.1$ $\mu$bar/s occurred at 850 and 500 mb, respectively. As the New Mexico storm occluded and the new Low at the point of the occlusion became prominent at 0000 GMT on the 21st, the maximum $\omega_F$ at 500 mb decreased to $-4.5$ $\mu$bar/s. By 0000 GMT March 22, the surface Low was less intense and the maximum 500-mb $\omega_F$ had further decreased to $-2.2$ $\mu$bar/s. Vertical motions and heights at 500 mb and surface features at one interim time, 1200 GMT on the 21st, are shown in figure 6. Strong subsidence (maximum 6.7 $\mu$bar/s at 500 mb) was centered southwest of the storm, reflecting the prominent ridge which followed the Low. However, as the cyclone weakened and the high pressure center over south central Canada failed to invade the central United States, the subsidence weakened. Once again, precipitation and radar depictions show good correlation with vertical motion fields.

A comparison between 0000 GMT (figs. 2 and 3) and 1200 GMT (fig. 6) charts on the 21st reveals a basic inconsistency: Despite the fact that the 500-mb Low deepened and the surface Low remained unchanged, the maximum upward motion decreased from $-4.6$ to $-3.9$ $\mu$bar/s. While this could be within the range of likely error, it is also probable that a representative 1200 GMT $\omega_F$ maximum is not shown because missing wind data made computations of $\omega$ impossible at Dayton, Ohio; Pittsburgh, Pa.; Washington, D.C.; Nashville, Tenn.; and Greensboro, N.C. The analysis in this part of the region is based on surrounding stations and the author's judgment about the continuity of the $\omega_F$ field. Although the author feels that the analysis is quite reasonable, a realistic maximum has probably been missed. A reasonable extrapolation of the isopleth field would lead to a maximum nearer $-6.5$ $\mu$bar/s, rather than $-3.9\mu$bar/s. This demonstrates the need for supplementing missing wind data, a problem not examined in this study.

The cross sections (fig. 5) likewise reveal reasonable correlation with circulation features. At 0000 GMT, March 18, the vertical motions were generally weak, reflecting the absence of major cyclone development. Subsidence is largely restricted to a dome below 600 mb over the large dominating high pressure system. Above and to the northeast and southwest, weak upward motion prevails. By 0000 GMT on the 21st the prominent cyclone development gave rise to substantially larger upward motions over a more extensive area. The two centers agree well with the two surface Lows and the 500-mb Low, prominent at this time.

## 5. COMPARISON OF KINEMATIC AND NUMERICAL VERTICAL MOTIONS

Discussions in the introduction and those of Miller and Panofsky (1958) indicate that the kinematic and numer-

TABLE 5.—*Comparison of adjusted kinematic ($\omega_F$) and NMC ($\omega_N$) numerical vertical motions. Weather classes and tabulated numbers are derived as in table 2.*

| | | Total up | | | Total down | | |
|---|---|---|---|---|---|---|---|
| $\omega_F$ | 0–3 | 29 | | (83) | 53 | | (183) |
| | 7–8 | 50 | 71 | (146) | 41 | 47 | (139) |
| | Precip. | 21 | | (61) | 6 | | (21) |
| $\omega_N$ | 0–3 | 26 | | (75) | 56 | | (191) |
| | 7–8 | 53 | 74 | (153) | 39 | 44 | (132) |
| | Precip. | 21 | | (63) | 5 | | (19) |

TABLE 6.—*Comparative statistics for 1200* GMT *Mar. 21, 1962 (this study) and 1200* GMT *Apr. 13, 1964 (Krishnamurti 1968b, Krishnamurti and Moxim 1971). Vertical motion units: µbar/s. Distance units: n.mi.*

| | $\omega_F$ | $\omega_Q$ | $\omega_C$ |
|---|---|---|---|
| Maximum upward | −6.5* | −7* | −14* |
| Maximum downward | 6.7 | 8* | 3* |
| Location of maximum up relative to surface Low | 300 ENE | 180 N | 135 N |
| Relative to 500-mb Low | 375 E | 260 NE | 280 ENE |
| Location of maximum down relative to surface Low | 540 SW | 120 S | 270 S |
| Relative to 500-mb Low | 490 SW | 320 SE | 430 SE |

*Estimated by extrapolation from highest value isopleth

ical methods are superior to other commonly used techniques for computing vertical motions. It would, of course, also be of great interest to know if either the kinematic or numerical method is consistently superior to the other. The following discussion does not attempt to settle this important issue, but rather serves as a preliminary analysis of the comparability of corrected kinematic and numerical estimates.

For direct comparison, 600-mb numerical $\omega$ computations ($\omega_N$) for the period of this study were read from NMC vertical motion charts. NMC employed the two-level mesh model (Ellsaesser 1960), which utilized a diagnostic $\omega$ equation derived from the adiabatic thermodynamic equation and dependent on the time derivative of the 850- to 500-mb thickness. The latter was obtained from a quasi-geostrophic formulation of the vorticity equation. Although this computational procedure differs from that normally used for the omega equation, the two are based on the same equations and physical assumptions. A particularly notable feature of the NMC computations is their consistently small magnitudes, seldom exceeding 2µbar/s.

Initial $\omega_N$ values were read at synoptic reporting stations and recorded by categories as in table 2. Unfortunately, the number of cases of $\omega_N$ in each category differed so greatly from $\omega_F$ that the only meaningful comparison possible was for the collective categories of total upward and downward motion. The comparative results for $\omega_F$ and $\omega_N$ are given in table 5. Although the differences are not great, the tabulated percentages indicate a slightly better performance from $\omega_N$. However, the consistently small magnitudes of $\omega_N$, a statistic not accounted for in table 5, decrease their general utility for diagnostic studies. Only 15 cases occurred with values greater than 2 µbar/s with only one case greater than 3 µbar/s. These almost certainly represent sizable underestimates of vertical motion, particularly in cases of well-developed cyclones. Considering both the results in table 5 and the ability of $\omega_F$ to yield values of more realistic magnitude, the author feels that the adjusted kinematic vertical motions are, in general, somewhat better for diagnostic analyses than the NMC numerical computations for this period.

Numerical estimates with magnitudes comparable to those of this study have been computed with the omega equation (O'Neill 1966, Krishnamurti 1968b, Krishnamurti and Moxim 1971). However, direct comparison with these studies is impossible because different periods are considered. Rather, the following discussion will only seek to compare major features of the numerical and kinematic computations. Direct comparisons between adjusted kinematic vertical motions and estimates provided from the omega equation for the same period are clearly needed and are currently being investigated by the author.

For this discussion, the map time 1200 GMT March 21 is considered because it most closely resembles, in state of development as well as geographical location, the case studied by Krishnamurti. Depicted in figure 6 are sea-level and 500-mb analyses for 1200 GMT, Mar. 21, 1962 and the comparative analysis from Krishnamurti (1968b) for 1200 GMT, Apr. 13, 1964. Superimposed on the upper air charts are corresponding vertical motion fields. On the March 21 chart, $\omega_F$ is shown. Two 500-mb charts are provided for Krishnamurti's case, one with a quasi-geostrophic field ($\omega_Q$) and the other with vertical motions ($\omega_C$) computed from a more complex model of the omega equation that considers 13 forcing functions, including friction, sensible heating, and release of latent heat (Krishnamurti and Moxim 1971). Earlier it was noted that 1200 GMT, March 21 was hampered by missing data, but that an extrapolated maximum of −6.5 µbar/s near Pittsburgh seemed reasonable.

Table 6 provides a summary of statistics derived from figure 6. All of the studies verify that vertical motions well in excess of 3 µbar/s can be expected with well-developed cyclones. Also comparable is the spread between maximum upward and downward motion of 13.2, 15, and 17µbar/s for $\omega_F$, $\omega_Q$, and $\omega_C$, respectively, although important differences exist in the individual magnitudes. The larger upward motions for the estimates derived from the omega equation can be partially explained by differences in the intensity of the Lows. On March 21, the surface Low minimum sea-level pressure reached 986 mb, while the minimum 500-mb height was about 5400 m. The corresponding values for Krishnamurti's case were between 975 and 980 mb and 5300 and 5350 m. A further notable difference between $\omega_F$ and the other estimates lies in the location of the maximum upward motion center relative to the surface Low. In both of the fields generated by the omega equation, this center is located north of the surface Low, while the $\omega_F$ maximum occurs to the east-northeast. This could be attributed to a major Canadian High

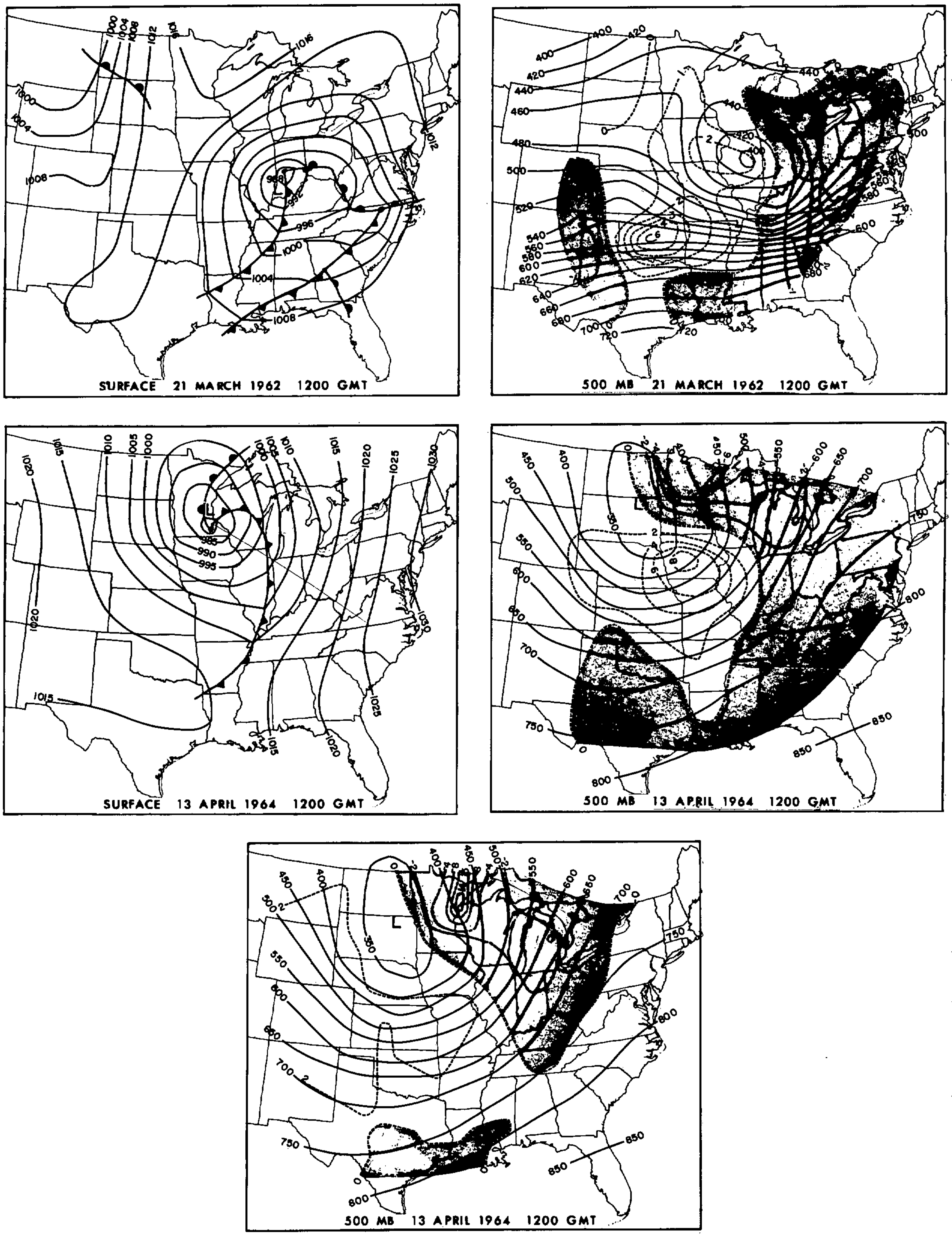


FIGURE 6.—Sea-level synoptic, 500-mb contour (m, initial 5 omitted), and vertical motion (dashed lines) analyses. Top: from this study; middle: from Krishnamurti's (1968*b*) quasi-geostrophic model; and bottom: from Krishnamurti and Moxim's (1971) complex model.

located north of the Low on March 21. A similar high pressure center was located well east of this position in Krishnamurti's case. Also in the latter case, a high pressure ridge invaded from the west and moved to a position south of the cyclone, compared with the southwesterly position indicated for March 21. This probably accounts for the more southerly and easterly position of the maximum subsidence for Krishnamurti's period. Thus, on a qualitative basis similarities in the $\omega$ fields are present, while important differences can be at least partially explained by differences in the synoptic situations. Certainly, the comparison is sufficient to indicate that corrected kinematic vertical motions are comparable to those obtained from the omega equation.

## 6. SUMMARY

The intent of this paper has been to analyze kinematic vertical motions in terms of their errors, relationships to observed synoptic features, and comparability to numerical estimates. Many of the discussions have been quite general in nature and have emphasized those features of the kinematic estimates that seemed most realistic, features that are predominant in the results. As is invariably the case with vertical motion studies, a close examination of the tables and figures will reveal displeasing features in the $\tilde{\omega}$ fields, evidence of the need for further efforts to improve vertical motion estimates.

To summarize, the following represent major conclusions of the study:

1. The computational scheme utilized for divergence computations does not reduce the cumulative bias error to acceptable levels at individual stations. Thus, a scheme to produce adjustments in kinematic $\omega$ estimates is needed.
2. Tests on the two adjustment techniques indicate that, for the period of this study, $\omega_F$ estimates are generally better, with both $\omega_F$ and $\omega_L$ showing improvement over the original kinematic estimates.
3. Precipitation, radar echoes, and general pressure distributions correlate well with $\omega_F$ fields.
4. The performance of $\omega_F$ was in general somewhat better than the NMC numerical estimates for this period. On a qualitative basis, corrected kinematic vertical motions are comparable to those obtained from formulations of the omega equation.

### ACKNOWLEDGMENTS

The author is indebted to Drs. E. M. Agee and D. G. Vincent of Purdue University and J. J. O'Brien of Florida State University for their helpful suggestions on this paper. The author also acknowledges the support provided for the original vertical motion computations at the University of Wisconsin by ESSA Grant WBG 52 and the Wisconsin Alumni Research Foundation. The research reported in this paper was supported by the Atmospheric Sciences Section, National Science Foundation, under Grant GA-10933.

### REFERENCES

Battan, Louis J., "Some Observations of Vertical Velocities and Precipitation Sizes in a Thunderstorm," *Journal of Applied Meteorology*, Vol. 3, No. 4, Aug. **1964**, pp. 415–420.

Bullock, Ben R., Horn, Lyle H., and Johnson, Donald R., "The Contribution of Infrared Cooling to the Vertical Motion Field and Its Implication in Atmospheric Energetics," *Monthly Weather Review*, Vol. 97, No. 5, May **1969**, pp. 371–381.

Cressman, George P., "A Three-Level Model Suitable for Daily Numerical Forecasting," *National Meteorological Center Technical Memorandum* No. 22, U.S. Department of Commerce, Weather Bureau, Washington, D.C., **1963**, 22 pp.

Danard, Maurice B., "On the Influence of Released Latent Heat on Cyclone Development," *Journal of Applied Meteorology*, Vol. 3, No. 1, Feb. **1964**, pp. 27–37.

Danielsen, Edwin F., "Research in Four-Dimensional Diagnosis of Cyclonic Storm Cloud Systems," *Scientific Report* No. 1, Contract No. AF19(628)-4762, Department of Meteorology, Pennsylvania State University, University Park, Jan. **1966**, 53 pp.

Duvedal, T., "Upper-Level Wind Computation With Due Regard to Both the Refraction of Electromagnetic Rays and the Curvature of the Earth," *Geophysica*, Vol. 8, No. 2, Helsinki, Finland, **1962**, pp. 115–124.

Ellsaesser, Hugh W., "JNWP Operational Models," *Joint Numerical Weather Prediction Office Note* No. 15, revised edition, U.S. Department of Commerce, Weather Bureau, Washington, D.C., Oct. **1960**, 33 pp.

Fankhauser, James C., "Convective Processes Resolved by a Mesoscale Rawinsonde Network," *Journal of Applied Meteorology*, Vol. 8, No. 5, Oct. **1969**, pp. 778–798.

Kreitzberg, Carl W., "The Mesoscale Wind Field in an Occlusion," *Journal of Applied Meteorology*, Vol. 7, No. 1, Feb. **1968**, pp. 53–67.

Krishnamurti, T. N., "A Diagnostic Balance Model for Studies of Weather Systems of Low and High Latitudes, Rossby Number Less Than 1," *Monthly Weather Review*, Vol. 96, No. 4, Apr. **1968***a*, pp. 197–207.

Krishnamurti, T. N., "A Study of a Developing Wave Cyclone," *Monthly Weather Review*, Vol. 96, No. 4, Apr. **1968***b*, pp. 208–217.

Krishnamurti, T. N., and Moxim, Walter J., "On Parameterization of Convective and Nonconvective Latent Heat Release," *Journal of Applied Meteorological*, Vol. 10, No. 1, Feb. **1971**, pp. 3–13.

Lateef, M. A., "Vertical Motion, Divergence, and Vorticity in the Troposphere Over the Caribbean, August 3–5, 1963," *Monthly Weather Review*, Vol. 95, No. 11, Nov. **1967**, pp. 778–790.

Miller, Albert, and Panofsky, Hans Arnold, "Large-Scale Vertical Motions and Weather in January, 1953," *Bulletin of the American Meteorological Society*, Vol. 39, No. 1, Jan. **1958**, pp. 8–13.

O'Brien, James J., "Alternative Solutions to the Classical Vertical Velocity Problem," *Journal of Applied Meteorology*, Vol. 9, No. 2, Apr. **1970**, pp. 197–203.

O'Neill, Thomas H. R., "Vertical Motion and Precipitation Computations," *Journal of Applied Meteorology*, Vol. 5, No. 5, Oct. **1966**, pp. 595–605.

Panofsky, Hans Arnold, "Large-Scale Vertical Velocity and Divergence," *Compendium of Meteorology*, American Meteorological Society, Boston, Mass., **1951**, pp. 639–646.

Smith, Phillip J., and Horn, Lyle H., "A Computational Study of the Energetics of a Limited Region of the Atmosphere," *Tellus*, Vol. 21, No. 2, Stockholm, Sweden, **1969**, pp. 193–210.

Smith, Phillip J., Horn, Lyle H., and Johnson, Donald R., "Energy Equations and Their Application to a Limited Region of the Atmosphere," *Studies of Large Scale Atmospheric Energetics, Annual Report*, ESSA Grant WBG 52, Department of Meteorology, The University of Wisconsin, Madison, Dec. **1967**, pp. 1–36.

Thompson, Philip Duncan, *Numerical Weather Analysis and Prediction*, Macmillan Co., New York, N.Y., **1961**, 170 pp.

White, Robert M., and Saltzman, Barry, "On Conversions Between Potential and Kinetic Energy in the Atmosphere," *Tellus*, Vol. 8, No. 3, Stockholm, Sweden, Aug. **1956**, pp. 357–363.

Wiin-Nielsen, A., "On Energy Conversion Calculations," *Monthly Weather Review*, Vol. 92, No. 4, Apr. **1964**, pp. 161–167.

*[Received January 11, 1971; revised April 5, 1971]*